Supplementary Methods, Clinical Information, Tables, and Figure Legends

Clonality Analysis and Sequencing

Read alignments were performed using a pipeline implemented in the Genome Modeling System [1] using the Common Workflow Language (CWL) [2]. Each run was executed on a compute cluster using Toil [3] as the workflow execution engine and platform LSF (IBM) as the job scheduler. Briefly, paired 2x150 bp reads were aligned to the human reference genome (version GRCh38) that had been supplemented with a list of cancer associated viral genome sequences including HTLV-1 (NC_001436.1 / AF033817.1) obtained from the NCI Genomic Data Common reference and decoy sequences obtained from the 1000 genomes project [4]. Alignments were performed with bwa mem version 0.7.15 (r1140) using default parameters except: '-K 100000000 -t 8 -Y -p'. The resulting alignment file was position sorted using SamBlaster [5] and duplicate reads were marked using Picard MarkDuplicates [6]. Sorted alignment files were indexed with samtools index [7]. Reads alignments were filtered to identify read pairs where one read of the pair aligned to the HTLV-1 genome and the other aligned a human genome reference sequence. Next the alignment start sites of all read alignments corresponding to the human reference genome were extracted and stored in a .bed format. Every human chromosome of the human reference genome was divided into 1000 bp segments using bedtools makewindows [8,9]. The number of alignment start positions falling within each 1000 bp segment were then determined using bedtools intersect. The counts for each region of the genome supporting an integration site were summarized in a table and normalized to account for differences in sequencing depth across the samples. The percentage of reads supporting a particular site was compared to the count of all HTLV integration site reads. Top integration sites were manually reviewed and counts for adjacent genome segments representing the same actual integration site were merged. These data were summarized to create Fig S7. Genomic DNA from patient samples was submitted to Invivoscribe for TRB and TRG gene rearrangement analysis and quantitation and genomic DNA from patient 3 was processed for common genomic substitutions using the "*Nexcourse Complete*" platform through Genoptix.

References

1. Griffith M, Griffith OL, Smith SM, et al. Genome modeling system: a knowledge management platform for genomics. *PLoS Computational Biology*. 2015;11:e1004274.
2. Chapman B, Chilton J, Heuer M, et al. Common Workflow Language, v1.0. In: Amtstuz P, Crursoe MR, Tijanic N eds; 2016.
3. Vivian J, Rao AA, Nothaft FA, et al. Toil enables reproducible, open source, big biomedical data analyses. *Nature Biotechnology*. 2017;35:314-316.
4. The Genomes Project C, Auton A, Abecasis GR, et al. A global reference for human genetic variation. *Nature*. 2015;526:68.
5. Faust GG, Hall IM. SAMBLASTER: fast duplicate marking and structural variant read extraction. *Bioinformatics*. 2014;30:2503-2505.
6. Van der Auwera GA, Carneiro MO, Hartl C, Poplin R, Del Angel G, Levy-Moonshine A, Jordan T, Shakir K, Roazen D, Thibault J, Banks E, Garimella KV, Altshuler D, Gabriel S, DePristo MA. From FastQ data to high confidence variant calls: the Genome Analysis Toolkit best practices pipeline. Curr Protoc Bioinformatics. 2013;43:11.10.1-33..
7. Li M, Kesic M, Yin H, Yu L, Green PL. Kinetic analysis of human T-cell leukemia virus type 1 gene expression in cell culture and infected animals. *Journal of Virology*. 2009;83:3788-3797.
8. Quinlan AR, Hall IM. BEDTools: a flexible suite of utilities for comparing gneomic features. *Bioinformatics*. 2010;26:841-842.
9. Quinlan AR. BEDTools: the Swiss-Army tool for genome feature analysis. *Current Protocols in Bioinformatics*. 2014;47:11.12.11-34.

Genes sequenced by Genoptix for Patient 3

ABL1
ABL2
AKT1
AKT2
AKT3
ALK
APC
AR
ARAF
ARHGEF1
ARID1A
ARID2
ASXL1
ATM
ATRX
AXL
B2M
BAP1
BCL2
BCL2L11
BCL6
BCOR
BIRC3
BRAF
BRCA1
BRCA2
BTK
CALR
CARD11
CBL
CCND1
CCND2
CCND3
CCNE1
CD274
CD33
CD79A
CD79B
CDH1
CDK2
CDK4
CDK6
CDKN1B
CDKN2A
CDKN2B
CEBPA

Genes sequenced for all patients

IRF4
PLCG1
CARD11
CD28
PRDM1
HLA-A
TP53
CDKN2A
GATA3
TBL1XR1
NOTCH1
CEBPA
BCL11B
GPR183
PAK2
DLG1
CD247
SYNCRIP
NRXN3
CD58
VAV1
HLA-B
ATXN1
PDCD1
CD274
PDL1
ARID2
COPS4
FAS
CELF2
POT1
CBLB
IRF2BP2
TET2
IKZF2
PRKCB
CCR7
CCR4
STAT3
RHOA

CHD1
CHEK2
CIC
CIITA
CREBBP
CRLF2
CSF1R
CSF3R
CTCF
CTNNB1
CXCR4
DAXX
DDR2
DDX3X
DDX41
DIS3
DNMT3A
EBF1
EGFR
EGR1
EIF1AX
EP300
EPCAM
EPHA2
EPOR
ERBB2
ERBB3
ERBB4
ESR1
ETNK1
ETV6
EWSR1
EZH2
FAM46C
FAS
FAT1
FBXW7
FGF19
FGFR1
FGFR2
FGFR3
FLT1
FOXO1
FUBP1
GAB2
GATA2
GATA3

GNA11
GNA13
GNAI2
GNAQ
GNAS
GNB1
H3F3A
HIF1A
HIST1H1E
HNF1A
HRAS
ID3
IDH1
IDH2
IGF1R
IKBKB
IKZF1
IKZF3
IRAK4
ITPKB
JAK1
JAK2
JAK3
KDR
KEAP1
KIT
KLF2
KRAS
MALT1
MAP2K1
MAP2K2
MAP2K4
MAP3K1
MAP3K14
MAP3K9
MAPK1
MCL1
MDM2
MDM4
MED12
MEF2B
MET
MITF
MLH1
KMT2D
MPL
MSH2

MSH6
MTOR
MYC
MYCN
MYD88
NF1
NF2
NFKBIE
NOTCH1
NOTCH2
NOTCH3
NPM1
NRAS
NT5C2
NTRK1
NTRK2
NTRK3
P2RY8
PALB2
PBRM1
PDGFRA
PDGFRB
PHF6
PIK3CA
PIK3CD
PIK3R1
PIM1
PLCG1
PLCG2
PMS2
POLE
POT1
PPM1D
PRDM1
PRPS1
PTCH1
PTEN
PTPN11
RAC1
RAD21
RB1
REL
RET
RHEB
RHOA
RICTOR
RIPK1

RIT1
RNF43
ROS1
RPS15
RUNX1
S1PR2
SAMHD1
SETBP1
SETD2
SF3B1
SGK1
SH2B3
SMAD4
SMARCB1
SMC1A
SMC3
SMO
SOCS1
SOX2
SPEN
SPOP
SRSF2
STAG2
STAT3
STAT5B
STAT6
STK11
TBL1XR1
TCF3
TERT
TET2
TGFBR1
TGFBR2
TLR2
TNFAIP3
TNFRSF14
TP53
TRAF2
TRAF3
TSC1
TSC2
U2AF1
UBR5
VHL
WT1
XPO1
ZFHX4

ZMYM3
ZRSR2

Clinical Summary of Patients Participating on NCT02631746: Phase II Trial of Nivolumab in Treating Patients with HTLV-Associated T-Cell Leukemia/Lymphoma

Patient 1:

The patient was a 58-year-old female from Chile with long standing chronic subtype ATLL who had progressive worsening of multiple subcutaneous lesions and had approximately twenty palpable nodules on her extremities and torso that included several 5 centimeter tumors at the initiation of treatment. The patient's laboratory data at the start of protocol treatment were unremarkable with hemoglobin of 10.3 g/dL, platelet count of 160,000/mm^3, white blood cell count (WBC) of 4140/mm^3, absolute lymphocyte count (ALC) 190/mm^3, slightly elevated ALT 48 U/L, AST 36 U/L, alkaline phosphatase 177 U/L, and LDH 265 U/L.

Within the first week following her initial treatment the patient noted new warmth, swelling and tenderness of nearly all of her multiple cutaneous lesions. When seen prior to her planned second Nivolumab infusion 2 weeks after her initial treatment, the patient's physical exam confirmed her report and showed swelling, tenderness and increased warmth of her ATLL lesions compared to normal adjacent areas of skin. Laboratory results at this time showed a significant increase in her LDH (809 IU) and new elevations of total (1.3mg/dl) and direct bilirubin (0.7mg/dl), increased WBC 7880, ALC 510 and appearance of a new population of abnormal mononuclear cells that constituted 7% of her peripheral blood leukocytes.that resulted in holding her planned second and ultimately third doses of treatment. The patient was started on high dose corticosteroid treatment for presumptive immune related complications. The patient also began to complain of left upper quadrant abdominal discomfort and was noted to have new splenomegaly, This physical exam finding was confirmed by ultrasound and MRI of the abdomen that showed new splenomegaly (14.7 cm → 23cm), multiple splenic infarcts, but no evidence of hepatic or biliary drainage system abnormalities (Figure S1) and her corticosteroids were discontinued. Coincidental to these events, the patient was also noted to have a rapid increase in atypical appearing lymphocytes classic for ATLL cells in her peripheral blood (Figure S1). To clarify the nature of these developments, the patient had a biopsy of a cutaneous tumor, flow cytometry analysis of her peripheral blood cells and a biopsy of her spleen. Flow cytometry analysis, immunohistochemical and pathologic analysis of the tissue specimens showed that the patient had developed a new population of double $CD4^{neg}$ $CD8^{neg}$, strongly $CD25^+$, $CD3^+$ lymphocytes in the peripheral blood that constituted nearly all the cells in the biopsies of her cutaneous tumor and spleen. These lymphocytes were phenotypically distinct from the $CD3^{low}$ $CD4^+CD25^+$ ATLL cells the patient had prior to starting treatment (Figure S1). The patient had progressive increase in the WBC, absolute lymphocyte count and abnormal mononuclear cells, continued worsening of her skin lesion and splenic enlargement. The patient was taken off protocol for rapidly progressive disease on 4 April and began palliative radiation therapy to her spleen and most symptomatic skin lesions.

Date (2017)	24 FEB	9 MAR	16 MAR	23 MAR	30 MAR	7 APR
LDH (U/L)	286	809	1335	900	ND	ND
WBC/mm^3	3470	7880	11630	12000	31720	40660
ALC/mm^3	230	510	950	1090	2730	1320
Percent "Other cells"	<1%	ND	23.5%	ND	36.7%	38.8%
Total Bilirubin (mg/dL)	0.2	0.7	1.8	0.5	ND	ND
HTLV-1 Proviral DNA Load (copies/PBMC)	0.02	ND	ND	1.25	ND	ND

Patient 2

Patient 2 was a 54 year old Jamaican woman with a past medical history significant only for ATL. She presented with cutaneous manifestations that first developed in January, 2015. It was initially thought that she had mycosis fungoides, and she was subsequently diagnosed with smoldering ATLL when HTLV1 IgG was identified, and bone marrow biopsy demonstrated 5% involvement by malignant CD4+ cells approximately 2 years prior to joining the clinical trial. Her previous treatments included: clobetasol, imiquimod and topical mechlorethamine for which she had partial and intermittent clinical responses. Approximately 8 months prior to joining the clinical trial, she developed two large cutaneous lesions, one on the right neck, and one on the left flank requiring radiotherapy to 800 cGy once to each lesion. In addition to these lesions, she noted progressive skin lesions despite topical therapies, and she was referred for consideration of nivolumab.

Prior to study enrollment, the patient had computerized tomographic scans of the neck, chest, abdomen, and pelvis with no evidence of ATLL. Bone marrow biopsy was performed which demonstrated the presence ATLL in a variable cellular marrow with significant fibrosis, and 60% involvement of the cellular marrow component. PD-1 testing of the bone marrow biopsy was performed and staining was noted in 10-20% of lymphocytes, primarily in fibrotic regions of the biopsy. PD-L1 testing was also conducted on the bone marrow biopsy sample and demonstrated only focal staining of possible histiocytes, which was thought to be non-specific and also in the fibrotic region of the bone marrow. She received her first and only infusion of nivolumab on June 27, 2017. Four days later, the patient developed diffuse aches and flu-like symptoms. Two days after that, labs were drawn and she was noted to have a creatinine of 2.5 mg/dL with a normal calcium level. She was admitted to the hospital and her creatinine improved to 1.53 mg/dL without intervention by the next day and she was discharged and monitored as an outpatient. Her ALC increased from 8230 to 14100 between cycle 1, day 1 (C1D1) and C1D10, and was 11950 by C2D1 when she returned to the treating institution. Nivolumab was held due to grade 3 renal toxicity on C2D1 (July 11, 2017) and there was no change in her cutaneous lesions. Eight days later, on C2D9 the patient presented to her local hospital with nausea, vomiting, fatigue, and elevated calcium to 13.3 mg/dL. The patient was treated with fluids and pamidronate, and positron emission tomography scan on C2D14 demonstrated diffuse uptake throughout the skeleton, lymph nodes, and spleen and bone marrow biopsy demonstrated continued involvement by ATLL in a fibrotic marrow. She was removed from study and initiated on salvage chemotherapy with CHOEP (cyclophosphamide, doxorubicin, vincristine, etoposide, and prednisone) at her local hospital. After 6 cycles of chemotherapy, the patient had total resolution of all skin lesions and disease

on PET scan, and she completed a haploidentical allogeneic stem cell transplant in December 2017 and remains in remission as of last follow-up locally.

Date (2017)	27 JUNE	3 JULY	10 JULY	11 JULY	17 JULY
Creatinine (mg/dL)	0.86	1.53	1.48	1.43	1.21
Calcium (mg/dL)	9.5	12.2	11.0	9.6	12.2
LDH (U/L)	207 (ULN 190)	266 (ULN 250)	260 (ULN 250)	351 (ULN 190)	ND
WBC/mm^3	11900	16200	17000	14400	15500
ALC/mm^3	8230	9977	14100	11950	ND
Alkaline Phosphatase (U/L)	213	274	252	286	460
HTLV-1 Proviral DNA Load (copies/PBMC)	1.1	ND	ND	ND	ND

Patient 3

Patient 3 was a 41 year old male from Jamaica, who presented six months prior to involvement in the study with acute ATLL with lymphadenopathy, abdominal distention, hypercalcemia, and leukocytosis, with bone marrow and peripheral blood involvement by ATL. The patient received dose-adjusted etoposide, prednisone, vincristine, cyclophosphamide, and doxorubicin, combined with raltegravir and bortezomib for 6 cycles and had a near complete response. He has also received intrathecal methotrexate for CNS prophylaxis. Three months later the patient relapsed with a brain mass and biopsy was consistent with a recurrence of ATLL. He had minimal disease in the rest of his body. Subsequently, he received 1 cycle of high dose methotrexate for his CNS disease and had a prompt remission and was referred for the clinical trial.

During evaluation for nivolumab therapy, the brain magnetic resonance imaging showed stable or improved lesions from the previous scan, and computerized tomographic scans showed right lower lobe pulmonary nodules, mild hilar and subcarinal lymphadenopathy. A bone marrow showed 19% atypical T cells, expressing CD2, CD3, CD4, CD5, and CD25, but no atypical T cells in the peripheral blood. The first and only infusion of nivolumab was given on November 14, 2017. Fourteen days after nivolumab treatment, the patient developed hypercalcemia, elevated transaminases, and renal insufficiency, Peripheral blood flow cytometry showed 30% of nucleated cells to be atypical lymphoid cells with a similar phenotype as that noted in the bone marrow earlier, and computerized tomographic scan showed new splenomegaly, and worsening mesenteric, retroperitoneal, pelvic, and inguinal adenopathy, and the patient was taken off protocol. The patient was initiated on salvage chemotherapy with ifosfamide, carboplatin, and etoposide on Dec 2, 2017. He initially responded to salvage chemotherapy, but after 2 cycles his disease progressed further and in the next few months, the patient passed away in peace.

Date (2017)	14 NOV	21 NOV	28 NOV	2 DEC	18 DEC
Creatinine (mg/dL)	1.0	1.1	1.7	1.2	1.0
Calcium (mg/dL)	9.8	10.4	11.8	8.5	9.4
LDH (U/L)	318	584	1143	3518	525
WBC/mm^3	6900	9100	10600	41200	5500
ALC/mm^3	1600	2300	3200	17000	1000
Aspartate Amino-transaminase (U/L)	23	49	165	146	55
Alanine Amino-transaminase (U/L)	14	36	162	90	76
Alkaline Phosphatase (U/L)	83	134	402	324	153
Total Bilirubin (mg/dL)	0.9	0.4	1.0	21.7	1.5
HTLV-1 Proviral DNA Load (copies/PBMC)	0.28	ND	0.67	ND	ND

Table S1: TCR Gene Rearrangement -TRG Analysis

Rank	Sequence	Length	Merge count	V-gene	J-gene	% total reads	Cumulative %	CDR3 Sequence
1	TGGGTAAGACAAGCAACAAAGTGGAGGCAAGAAAG	144	90769	Vg10	JgP1	39.37	39.37	GCTGCGTATACCACTGGTTGGTTCAAGATA
2	AGAATCAGTAGAGGAAAGTATTTTACTTATGCAAGC/	139	33237	Vg3	JgP1	14.42	53.79	not found
3	GGAATCAGTCGAGAAAAGTATCATACTTATGCAAGC	144	23095	Vg8	JgP1	10.02	63.81	not found
4	GGAATCAGCCCAGGGAAGTATGATACTTACGGAAG	139	2219	Vg4	Jg1/2	0.96	64.77	GCCACCTCACACACGCCTAAGAAACTC
5	GGAATCAGCCCAGGGAAGTATGATACTTATGGAAG	148	2058	Vg4	JgP1	0.89	65.67	GCCACCTGGGATAGCGGGGGGACTGGTTGGTTCAAGATA
Sample	**1B**							
Total count	**453,436**							
CLONAL								
Rank	**Sequence**	**Length**	**Merge count**	**V-gene**	**J-gene**	**% total reads**	**Cumulative %**	**CDR3 Sequence**
1	TGGGTAAGACAAGCAACAAAGTGGAGGCAAGAAAG	144	396378	Vg10	JgP1	87.42	87.42	GCTGCGTATACCACTGGTTGGTTCAAGATA
2	AGAATCAGTAGAGGAAAGTATTTTACTTATGCAAGC/	139	14302	Vg3	JgP1	3.15	90.57	not found
3	GGAATCAGTCGAGAAAAGTATCATACTTATGCAAGC	144	10797	Vg8	JgP1	2.38	92.95	not found
4	GGAATCAGCCCAGGGAAGTATGATACTTATGGAAG	148	8857	Vg4	JgP1	1.95	94.91	GCCACCTGGGATAGCGGGGGGACTGGTTGGTTCAAGATA
5	TGGGTAAGACAAGCAACAAAGTGGAGGCAAGAAAG	148	588	Vg10	JgP1	0.13	95.03	not found
Sample	**2A**							
Total count	**460,599**							
CLONAL								
Rank	**Sequence**	**Length**	**Merge count**	**V-gene**	**J-gene**	**% total reads**	**Cumulative %**	**CDR3 Sequence**
1	GGAATCAGCCCAGGGAAGTATGATACTTATGGAAG	141	198027	Vg4	JgP	42.99	42.99	not found
2	AGAATCAGTAGAGGAAAGTATTTTACTTATGCAAGC/	141	179179	Vg3	Jg1/2	38.90	81.89	GCCACCTGGGACAGGCCGGGTAAGAAACTC
3	GGAGTCAGTCCAGGGAAGTATTATACTTACGCAAG	126	367	Vg2	none	0.08	81.97	not found
4	GGAATCAGTCGAGAAAAGTATCATACTTATGCAAGC	140	248	Vg8	JgP1	0.05	82.03	not found
5	GGAGTCAGTCCAGGGAAGTATTATACTTACGCAAG	129	245	Vg2	JgP2	0.05	82.08	not found
Sample	**3A**							
Total count	**393,715**							
CLONAL								
Rank	**Sequence**	**Length**	**Merge count**	**V-gene**	**J-gene**	**% total reads**	**Cumulative %**	**CDR3 Sequence**
1	GGAGTCAGTCCAGGGAAGTATTATACTTACGCAAG	126	139454	Vg2	none	35.42	35.42	not found
2	GGACTCAGTCCAGGAAAGTATTATACTCATACACCC	141	82516	Vg3	Jg1/2	20.96	56.38	not found
3	GGAGTCAGTCCAGGGAAGTATTATACTTACGCAAG	147	2864	Vg2	Jg1/2	0.73	57.11	not found
4	GGAGTCAGTCCAGGGAAGTATTATACTTACGCAAG	146	2792	Vg2	Jg1/2	0.71	57.81	not found
5	TGGGTAAGACAAGCAACAAAGTGGAGGCAAGAAAG	140	2596	Vg10	JgP1	0.66	58.47	not found
Sample	**3B**							
Total count	**340,978**							
CLONAL								
Rank	**Sequence**	**Length**	**Merge count**	**V-gene**	**J-gene**	**% total reads**	**Cumulative %**	**CDR3 Sequence**
1	GGAGTCAGTCCAGGGAAGTATTATACTTACGCAAG	126	166294	Vg2	none	48.77	48.7697153	not found
2	GGACTCAGTCCAGGAAAGTATTATACTCATACACCC	141	121295	Vg3	Jg1/2	35.57	84.3423916	not found
3	GGACTCAGTCCAGGAAAGTATTATACTCATACACCC	141	1070	Vg3	Jg1/2	0.31	84.6561948	GCCACCTGGGACAGGCGGGGGAGAAACTCT
4	GGAGTCAGTCCAGGGAAGTATTATACTTACGCAAG	143	952	Vg2	Jg1/2	0.28	84.9353917	not found
5	AGAATCAGTAGAGGAAAGTATTTTACTTATGCAAGC/	145	785	Vg3	Jg1/2	0.23	85.1656119	not found

Table S2: TCR Gene Rearrangement -TRB Analysis

Sample	**1A**							
Total count	**208,170**							
CLONAL								
Rank	**Sequence**	**Length**	**Merge count**	**V-gene**	**J-gene**	**% total reads**	**Cumulative %**	**CDR3 Sequence**
1	CCTTCCCATTTTAATTCACTGCCTTTGTCTTTTCCAA(	202	73946	Db2	Jb2-2	35.52	35.52	not found
2	GGAGGTGAGAAGGAAGCCCCCGGCCTGGTCCATA(	212	37587	Db1	Jb1-2	18.06	53.58	not found
3	TATTATAATGGAGAAGAGAGAGCAAAAGGAAACATT	174	16966	Vb9	Jb1-1	8.15	61.73	GCCAGCAGCGTACCTGGACAGGGGGGGAAAGCTTTC
4	CCTTCCCATTTTAATTCACTGCCTTTGTCTTTTCCAA(	201	14393	Db2	Jb2-1	6.91	68.64	not found
5	GGAGGTGAGAAGGAAGCCCCCGGCCTGGTCCATA(	262	6997	Db1	Jb2-5	3.36	72.00	not found
Sample	**1B**							
Total count	**360,431**							
CLONAL								
Rank	**Sequence**	**Length**	**Merge count**	**V-gene**	**J-gene**	**% total reads**	**Cumulative %**	**CDR3 Sequence**
1	CCTTCCCATTTTAATTCACTGCCTTTGTCTTTTCCAA(	202	231911	Db2	Jb2-2	64.34	64.34	not found
2	GGAGGTGAGAAGGAAGCCCCCGGCCTGGTCCATA(	212	81838	Db1	Jb1-2	22.71	87.05	not found
3	CCTTCCCATTTTAATTCACTGCCTTTGTCTTTTCCAA(	201	5810	Db2	Jb2-1	1.61	88.66	not found
4	TATTATAATGGAGAAGAGAGAGCAAAAGGAAACATT	174	4142	Vb9	Jb1-1	1.15	89.81	GCCAGCAGCGTACCTGGACAGGGGGGGAAAGCTTTC
5	GGAGGTGAGAAGGAAGCCCCCGGCCTGGTCCATA(	262	1663	Db1	Jb2-5	0.46	90.27	not found
Sample	**2A**							
Total count	**436,559**							
CLONAL								
Rank	**Sequence**	**Length**	**Merge count**	**V-gene**	**J-gene**	**% total reads**	**Cumulative %**	**CDR3 Sequence**
1	AATTATGAAGCCCAACAAGACAAATCAGGGCTGCC(	171	55944	Vb7-6	Jb2-3	12.81	12.81	GCCAGCAGCTTAGGCACAGATACGCAGTAT
2	TTCAATTATGAAGCCCAACAAGACAAATCAGGGCTG	174	10396	Vb7-6	Jb2-3	2.38	15.20	GCCAGCAGCTTAGGCACAGATACGCAGTAT
3	AATTATGAAGCCCAACAAGACAAATCAGGGCTGCC(	325	7558	Vb7-6	Jb2-3	1.73	16.93	not found
4	TTCAATTATGAAGCCCAACAAGACAAATCAGGGCTG	328	1258	Vb7-6	Jb2-3	0.29	17.22	not found
5	CAGAGGAAGGTCTGAAATTCATGGTTTATCTCCAGA	225	886	Vb18	Jb2-7	0.20	17.42	GCTCACCACCGGGACCGATAAGACCGAGCTCCTACGAGCA
Sample	**3A**							
Total count	**509,164**							
CLONAL								
Rank	**Sequence**	**Length**	**Merge count**	**V-gene**	**J-gene**	**% total reads**	**Cumulative %**	**CDR3 Sequence**
1	TTCAGTTCCTCTTTGAATACTTCAGTGAGACACAGA(	200	136306	Vb5-1	Jb2-3	26.77	26.77	CCAGCAGCTTGTGTGTGACAGGGAGCACAGATACGCAGTA
2	CTGAGATTGATCTACTACTCACAGATAGTAAATGAC	206	74698	Vb19	Jb2-1	14.67	41.44	not found
3	CCTTCCCATTTTAATTCACTGCCTTTGTCTTTTCCAA(	234	3872	Db2	Jb2-5	0.76	42.20	not found
4	TTCCAGAATGAAGCTCAACTAGACAAATCGGGGCT(	178	3647	Vb7-8	Jb1-4	0.72	42.92	GCCAGCAGTCGGGTCGCGGCTAATGAAAAACTGTTT
5	ATGGGCTGAGGCTGATCCATTACTCATATGGTGTTA	214	2960	Vb10-3	Jb1-2	0.58	43.50	not found
Sample	**3B**							
Total count	**415,226**							
CLONAL								
Rank	**Sequence**	**Length**	**Merge count**	**V-gene**	**J-gene**	**% total reads**	**Cumulative %**	**CDR3 Sequence**
1	TTCAGTTCCTCTTTGAATACTTCAGTGAGACACAGA(	200	160594	Vb5-1	Jb2-3	38.68	38.68	CCAGCAGCTTGTGTGTGACAGGGAGCACAGATACGCAGTA
2	CTGAGATTGATCTACTACTCACAGATAGTAAATGAC	206	129233	Vb19	Jb2-1	31.12	69.80	not found
3	AGGGCCTTCAGTTCCTCTTTGAATACTTCAGTGAGA	206	3897	Vb5-1	Jb2-3	0.94	70.74	CCAGCAGCTTGTGTGTGACAGGGAGCACAGATACGCAGTA
4	TTCAGTTCCTCTTTGAATACTTCAGTGAGACACAGA(	354	2493	Vb5-1	Jb2-3	0.60	71.34	not found
5	ACAAGGGCTGAGATTGATCTACTACTCACAGATAGT	213	2166	Vb19	Jb2-1	0.52	71.86	not found

Supplemental Figure Legends

Figure S1: Expansion of CD4-CD8-CD25+PD-1+ ATLL cells in the peripheral blood after nivolumab. Flow cytometry, CT, and blood counts charting the expansion of a CD4-CD8- (double negative) population of CD25+ atypical cells in the peripheral blood after nivolumab therapy. A quotation of the primary physican's report detailing the changing immunophenotype in this patient.

Figure S2. Post-relapse ATLL cells express PD-1 and are subject to PD-L1 induced growth inhibition. PD1 and PDL1 expression before and after nivolumab in Patient 3. Flow cytometry histograms of PD1 and PD1 stained K562 cells, BM biopsy obtained prior to nivolumab therapy, and CD4+CD7- cells obtained from the peripheral blood after nivolumab therapy in patient 3.

Figure S3: Reverse Phase Protein Array Analysis on PBMC from Patient 1
Reverse phase protein array analysis was used to quantitate 301 proteins and phosphoproteins in lysates of PBMC obtained before and after nivolumab therapy in Patient 1. The ratio (after/before) of normalized linear values obtained for each gene was calculated and all proteins undergoing > 3-fold increase or >2-fold decrease after nivolumab are shown. The TCR signaling pathway (red) is the most highly enriched pathway associated with the proteins elevated after nivolumab and ERB-B signaling (green) is most associated with the proteins decreased after nivolumab.

Figure S4. Mouse models of aggressive ATLL do not recapitulate rapid progression seen in patients. Nivolumab causes reduced white cell count, reduced human CD4 T cell count and reduced total human cells in PDX model. Mouse PD-1 antibody causes decreased tumor growth in Tax mice.Fewer human T cells expressing CD4, CD8 or CD27 are present in spleen of HTLV-1 infected humanized mice treated with nivolumab compared to PBS.

Figure S5: Increased Expression of checkpoints in ATLL. Data from an ATLL gene expression microarray study by Nakano was downloaded from the Gene Expression Omnibus at the NCBI (GEO accession: GSE33615). In the original study, RNA was extracted from PBMCs

isolated from patients with acute (n=26), chronic (n=20), lymphomatous (n=1), and smoldering (n=4) ATLL, and compared to RNA obtained from CD4+ cells from 21 normal subjects. In this study, values were normalized to actin (ACTB) then represented as fold-Patient 10 (a smoldering ATLL sample with the lowest proviral load in the study).

Figure S6: Immune response in chronic and smoldering forms of ATLL is similar to patients who achieve operational tolerance after allogeneic transplantation. Analysis of microarray data as described in Figure S7. Red bar represents the median. Genes shown are elevated ($p < 0.01$) in chronic and smoldering disease but not in normal patients or patients with acute ATL.

Figure S7: Human T-cell leukemia virus (HTLV) integration sites among 5 samples from 3 individuals. (A) The number of 1KB windows across the genome associated with HTLV reads, the total number of normalized HTLV associated reads, and the total number of mapped (aligned) reads are shown for each sample. (B) The percentage of HTLV reads for each sample associated with an integration site summing to 100%. Binned Sites represent grouped integration sites for which the percentage of HTLV reads was less than 1%. (C) The frequency of normalized HTLV reads associated with the top integration site for each of the three patients is shown in the context of the full chromosomes. The top integration sites occurred on chromosome 2 for two patients (002 and 003) and chromosome 20 for the third patient (001). Triangles represent the top integration site for each sample in terms of the frequency of HTLV reads. Colors for all samples remain the same for each panel in the figure.

Figure S1: Expansion of CD4-CD8-CD25+PD-1+ ATLL cells in the peripheral blood after nivolumab. Flow cytometry, CT, and blood counts charting the expansion of a CD4-CD8- (double negative) population of CD25+ atypical cells in the peripheral blood after nivolumab therapy. The patient had a history of HTLV-1 associated adult T-cell leukemia/lymphoma (ATLL). 95% of the lymphoid cells in the blood were abnormal T cells with the majority population (84% of lymphoid cells) expressing partial CD2 (45% positive), spectrum of CD3 from dim to predominately negative, bright CD5, bright CD25, CD45, and bright CD52, but negative for CD4, CD7, CD8, CD26, CD16, CD13, CD14, CD34, CD56, CD57, and TCR gamma delta. A minor sub-population (10.9% of the lymphoid cells) expressed CD2, dim CD3, CD4, spectrum of CD5 from bright to moderate, bright CD25, CD45, and bright CD52, but were negative for CD7, CD8, CD26, CD16, CD13, CD14, CD34, CD56, CD57, and TCR gamma delta. The immunophenotypic data was diagnostic of the patient's HTLV-1-associated adult T-cell leukemia and is consistent with the changing immunophenotype observed in recent specimens from this patient (decreasing CD3, decreasing CD4 and increasing CD5 expression in a sub-population). The neoplastic cells in the spleen were positive for CD3 (mostly cytoplasmic), double negative for CD4 and CD8, weakly and focally positive for PD-1 and show high proliferative rate as per MIB-1. The neoplastic cells in the spleen were positive for Atypical T-cells are strong and diffuse for CD3 and PD1. CD25 and CD30 are focally positive in a similar distribution. PDL1 is positive in the stroma and macrophages. CD20 highlighted rare B-cells in the dermis. The skin biopsy from 2010 was analyzed for PD-1, and only a subset of the atypical cells was positive for it in contrast with the current biopsy. CD3 (mostly cytoplasmic), double negative for CD4 and CD8, weakly and focally positive for PD-1 and show high proliferative rate as per MIB-1.

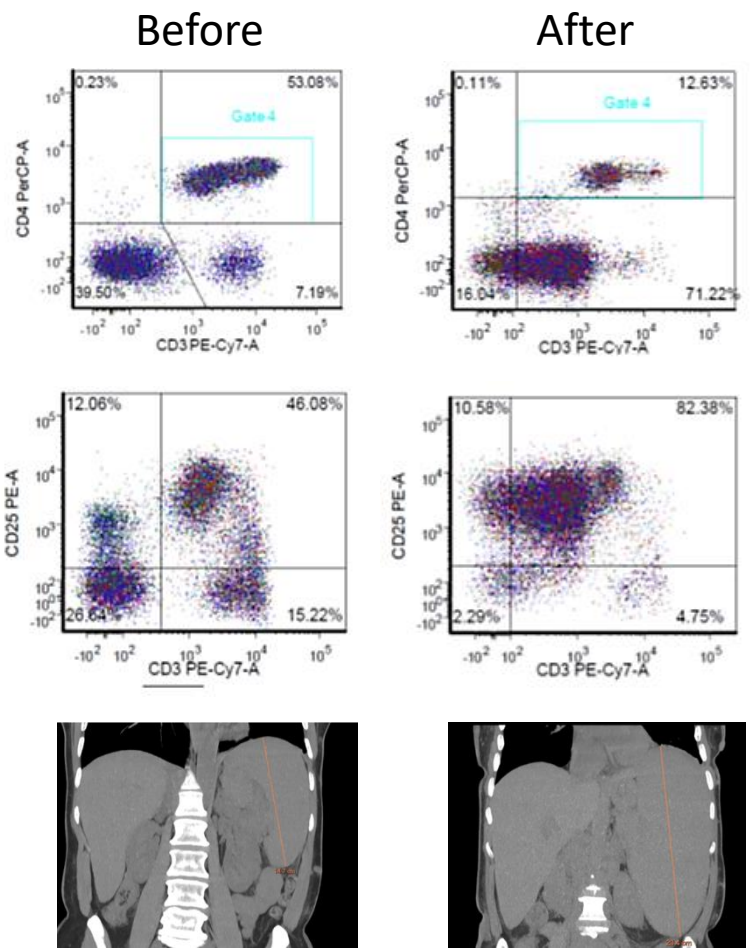

3470	**WBC/mm^3**	31720
230	**Absolute lymphocyte count/mm^3**	2730
-	**Percent "Other cells"**	36.7%

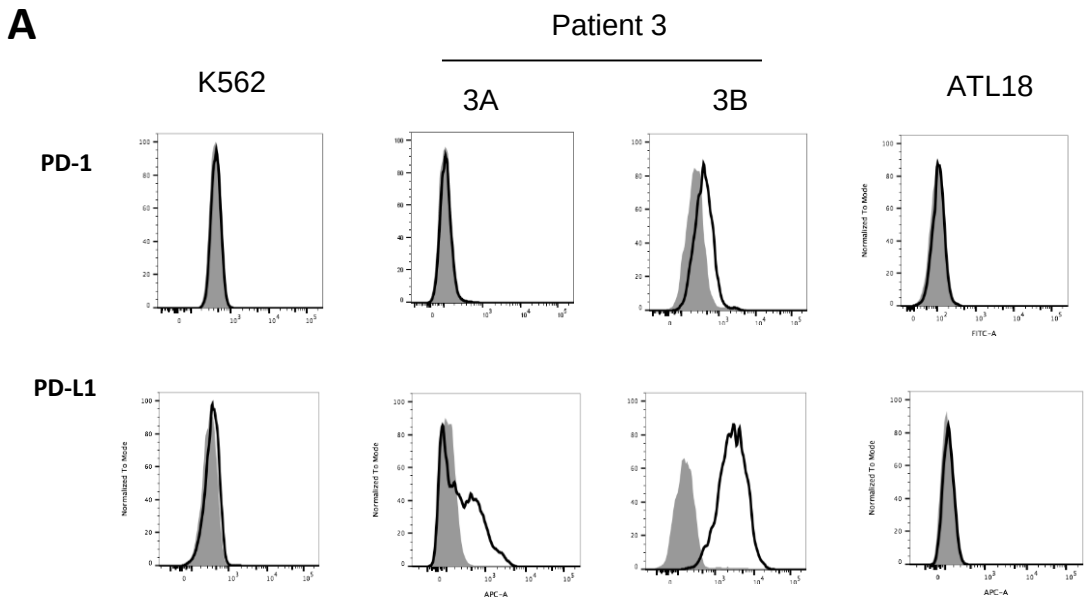

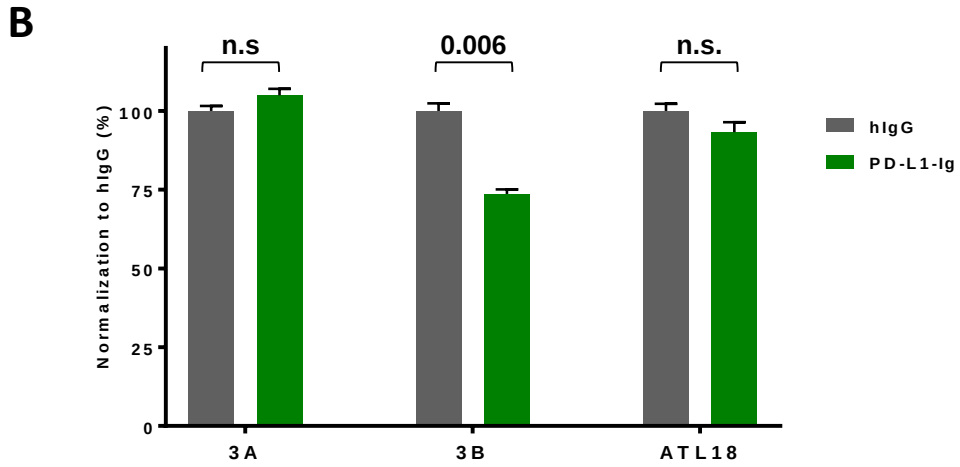

Figure S2. Post-relapse ATLL cells express PD-1 and are subject to PD-L1 induced growth inhibition.
A.Flow cytometry measurement of PD-1 and PD-L1 expression on leukemic cells from Patient 3 before (3A) and after (3B) Nivolumab treatment . K562, a negative control for PD-1 and PD-L1 staining. ATL18, an established ATLL cell line.3A, short-term (5 wk) culture from a bone marrow sample. 3B, total PBMCs. Analysis was gated on CD4+CD7- cells.
B.Effect of PD-L1-Ig on in vitro proliferation of ATLL cells was evaluated with the Cell Counting Kit – SK method. Two-tailed t-test was performed for pairwise comparisons as indicated. n.s., not signifiant.

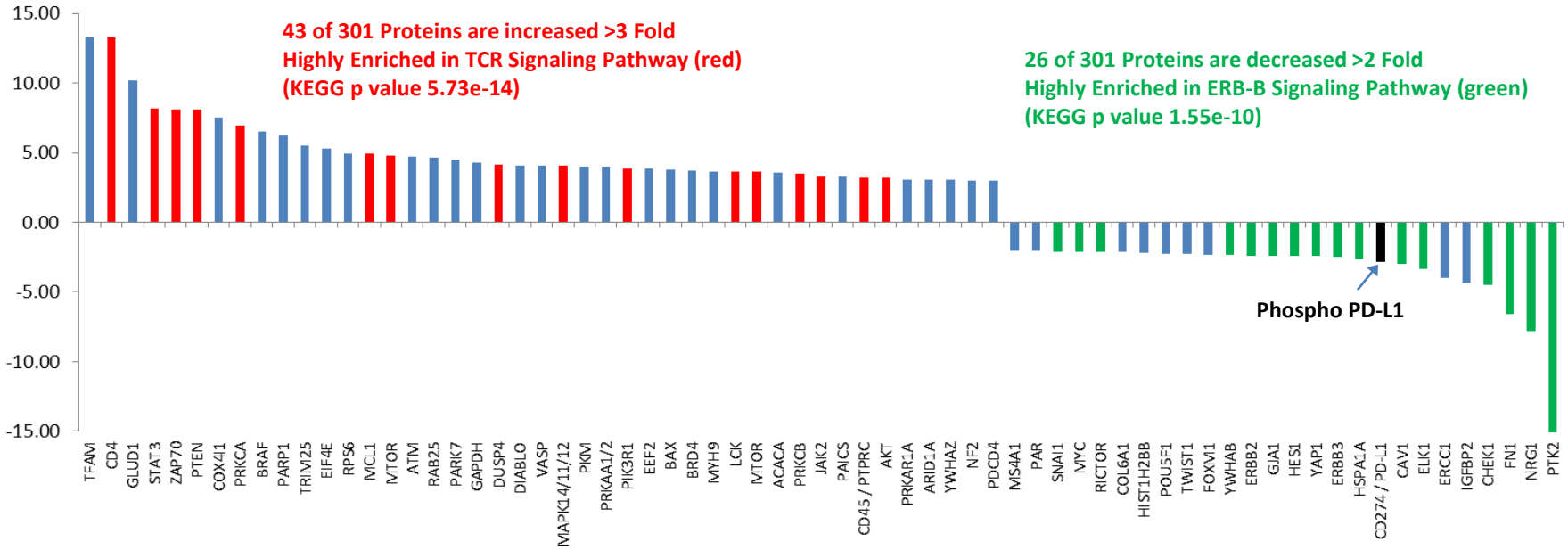

Figure S3: Reverse Phase Protein Array Analysis on PBMC from Patient 1

Reverse phase protein array analysis was used to quantitate 301 proteins and phosphoproteins in lysates of PBMC obtained before and after nivolumab therapy in Patient 1. The ratio (after/before) of normalized linear values obtained for each gene was calculated and all proteins undergoing > 3-fold increase or >2-fold decrease after nivolumab are shown. The TCR signaling pathway (red) is the most highly enriched pathway associated with the proteins elevated after nivolumab and ERB-B signaling (green) is most associated with the proteins decreased after nivolumab.

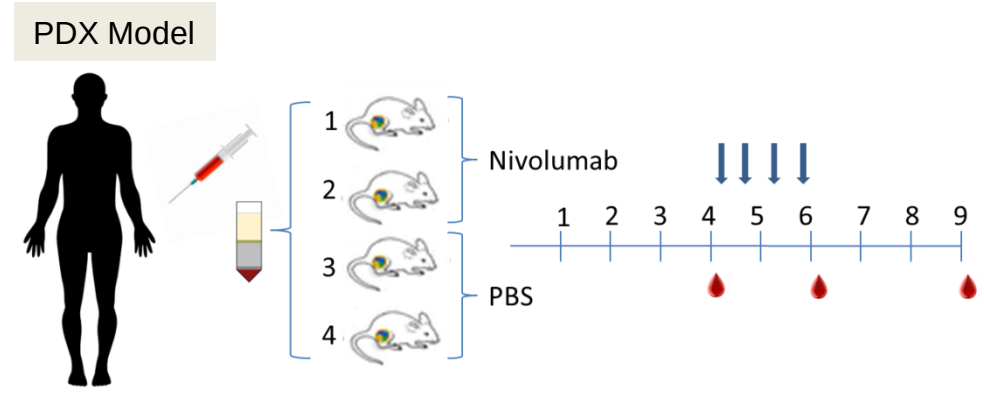

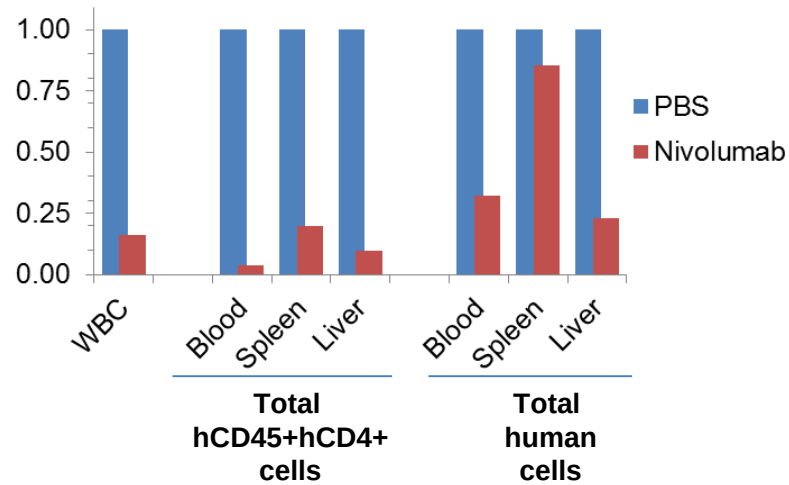

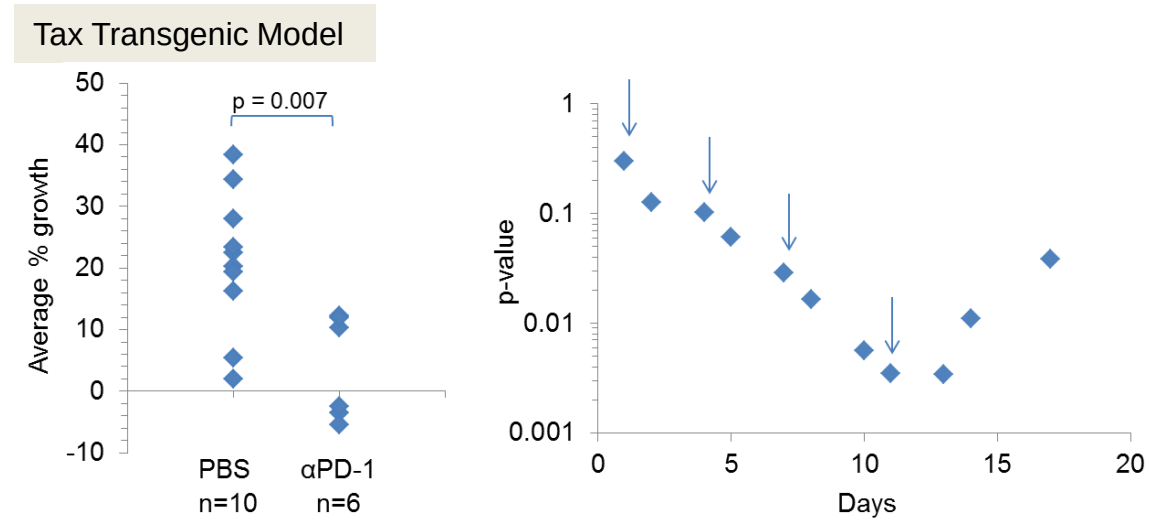

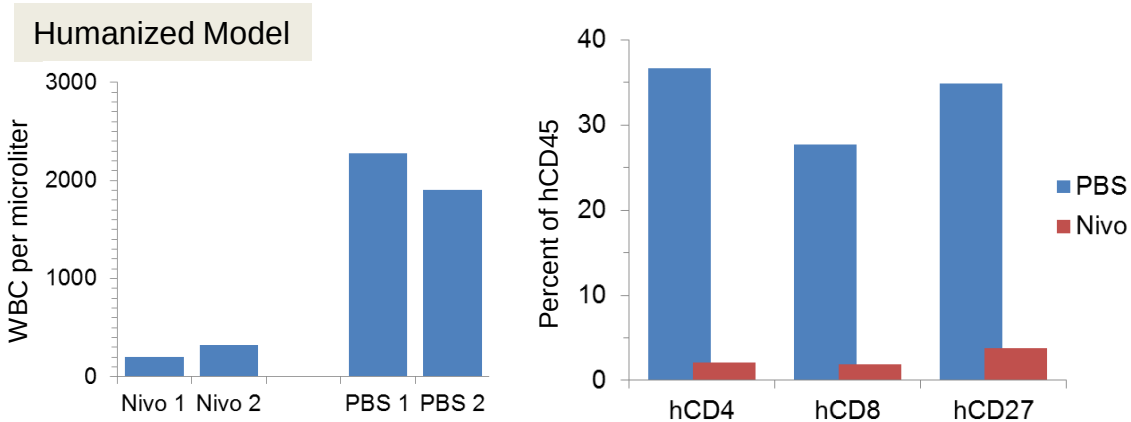

Figure S4. Mouse models of aggressive ATLL do not recapitulate rapid progression seen in patients
Nivolumab causes reduced white cell count, reduced human CD4 T cell count and reduced total human cells in PDX model.
Mouse PD-1 antibody causes decreased tumor growth in Tax mice.
Fewer human T cells expressing CD4, CD8 or CD27 are present in spleen of HTLV-1 infected humanized mice treated with nivolumab compared to PBS.

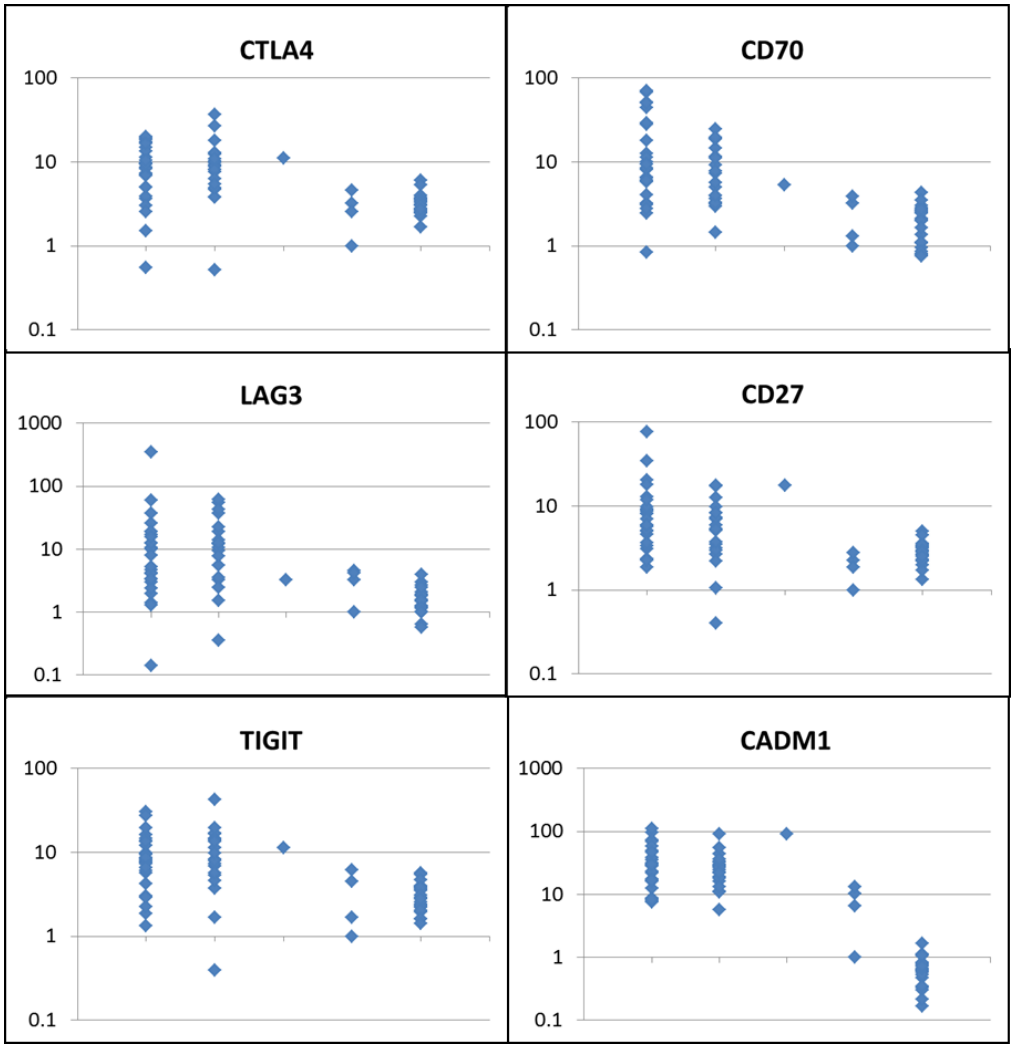

Columns Left to Right
Acute (n=26)
Chronic (n=20)
Lymphoma (n=1)
Smoldering (n=4)
Normal (n=21)

Figure S5: Increased Expression of checkpoints in ATLL. Data from an ATLL gene expression microarray study by Nakano was downloaded from the Gene Expression Omnibus at the NCBI (GEO accession: GSE33615). In the original study, RNA was extracted from PBMCs isolated from patients with acute (n=26), chronic (n=20), lymphomatous (n=1), and smoldering (n=4) ATLL, and compared to RNA obtained from CD4+ cells from 21 normal subjects. In this study, values were normalized to actin (ACTB) then represented as fold-Patient 10 (a smoldering ATLL sample with the lowest proviral load in the study).

Figure S6: Immune response in chronic and smoldering forms of ATLL is similar to patients who achieve operational tolerance after allogeneic transplantation. Analysis of microarray data as described in Figure S7. Red bar represents the median. Genes shown are elevated ($p < 0.01$) in chronic and smoldering disease but not in normal patients or patients with acute ATLL.

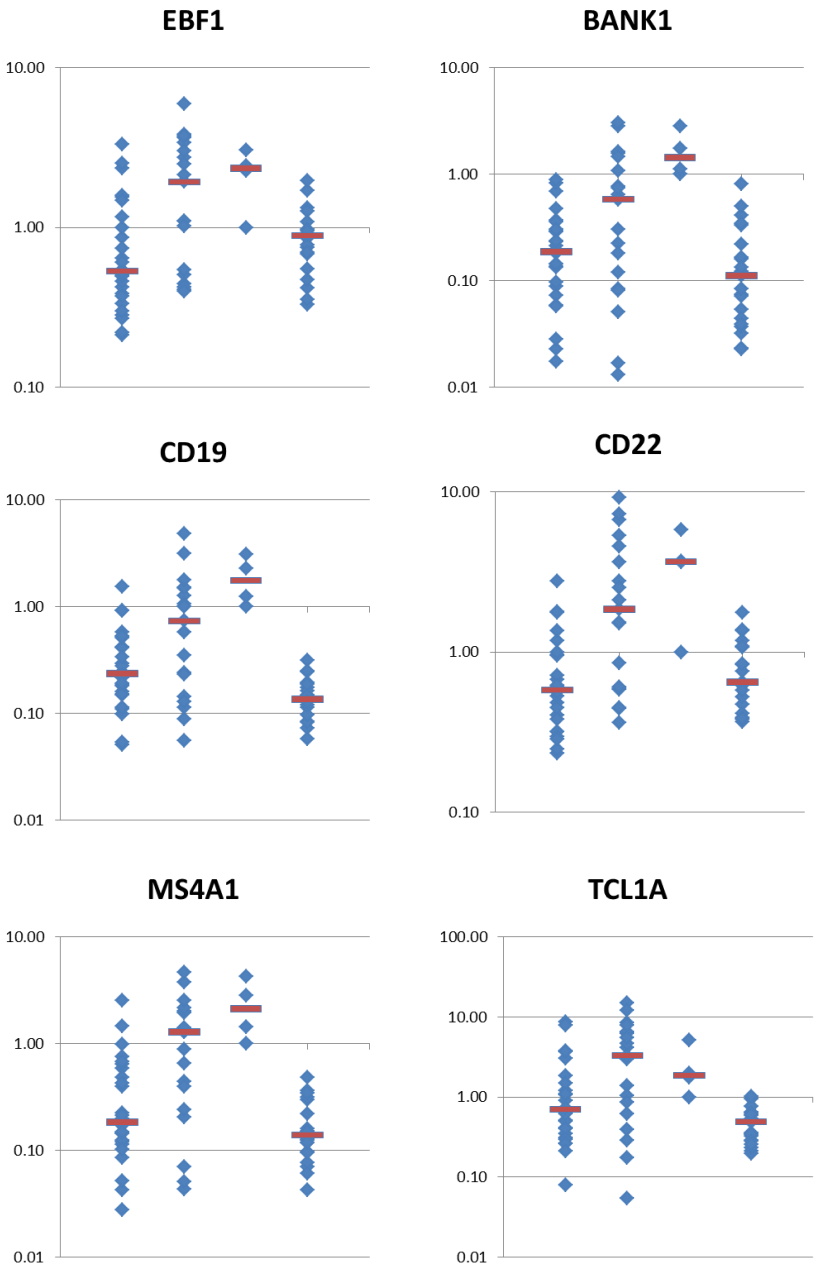

Columns Left to Right
- Acute (n=26)
- Chronic (n=20)
- Smoldering (n=4)
- Normal (n=21)

Figure S7: Human T-cell leukemia virus (HTLV) integration sites among 5 samples from 3 individuals. (A) The number of 1KB windows across the genome associated with HTLV reads, the total number of normalized HTLV associated reads, and the total number of mapped (aligned) reads are shown for each sample. (B) The percentage of HTLV reads for each sample associated with an integration site summing to 100%. Binned Sites represent grouped integration sites for which the percentage of HTLV reads was less than 1%. (C) The frequency of normalized HTLV reads associated with the top integration site for each of the three patients is shown in the context of the full chromosomes. The top integration sites occurred on chromosome 2 for two patients (002 and 003) and chromosome 20 for the third patient (001). Triangles represent the top integration site for each sample in terms of the frequency of HTLV reads. Colors for all samples remain the same for each panel in the figure.

:

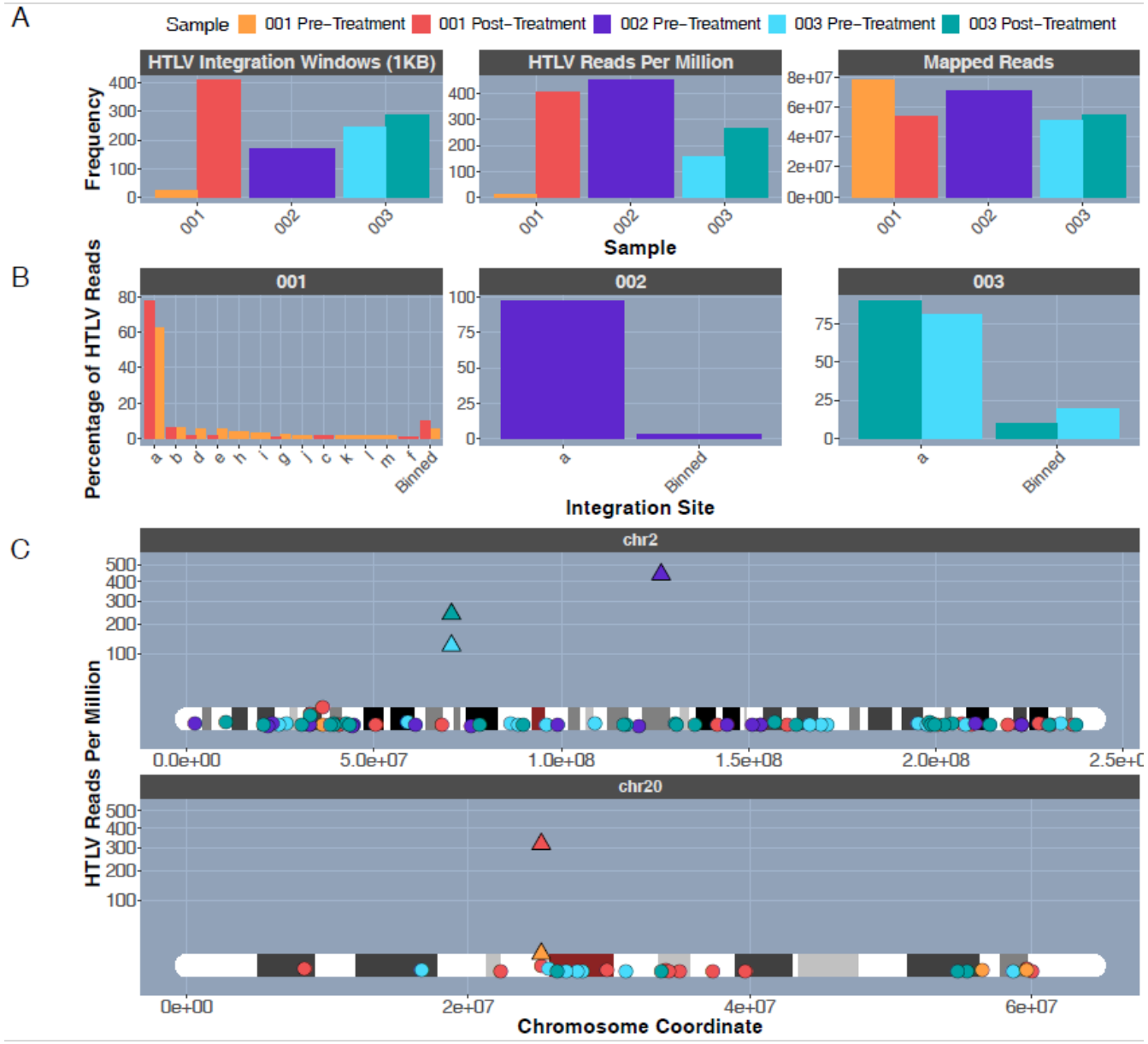

CONSORT
TRANSPARENT REPORTING of TRIALS

CONSORT 2010 Flow Diagram